

Tumour suppressor RNF43 is a stem-cell E3 ligase that induces endocytosis of Wnt receptors

Bon-Kyoung Koo¹, Maureen Spit^{2*}, Ingrid Jordens^{2*}, Teck Y. Low^{3,4}, Daniel E. Stange¹, Marc van de Wetering¹, Johan H. van Es¹, Shabaz Mohammed^{3,4}, Albert J. R. Heck^{3,4}, Madelon M. Maurice² & Hans Clevers¹

LGR5⁺ stem cells reside at crypt bottoms, intermingled with Paneth cells that provide Wnt, Notch and epidermal growth factor signals¹. Here we find that the related RNF43 and ZNRF3 transmembrane E3 ubiquitin ligases are uniquely expressed in LGR5⁺ stem cells. Simultaneous deletion of the two genes encoding these proteins in the intestinal epithelium of mice induces rapidly growing adenomas containing high numbers of Paneth and LGR5⁺ stem cells. *In vitro*, growth of organoids derived from these adenomas is arrested when Wnt secretion is inhibited, indicating a dependence of the adenoma stem cells on Wnt produced by adenoma Paneth cells. In the HEK293T human cancer cell line, expression of RNF43 blocks Wnt responses and targets surface-expressed frizzled receptors to lysosomes. In the RNF43-mutant colorectal cancer cell line HCT116, reconstitution of RNF43 expression removes its response to exogenous Wnt. We conclude that RNF43 and ZNRF3 reduce Wnt signals by selectively ubiquitinating frizzled receptors, thereby targeting these Wnt receptors for degradation.

The small intestinal epithelium self renews every 4–5 days, making it the fastest proliferating mammalian tissue. Crypt base columnar (CBC) cells² are small cycling cells residing between the terminally differentiated Paneth cells at crypt bottoms. We identified *Lgr5* as a marker for these cells and integrated an enhanced green fluorescent protein (EGFP)–internal ribosome entry site (IRES)–*creERT2* cassette into the locus. As shown by lineage tracing, LGR5⁺ cells generate all cell types of the epithelium over the lifetime of the animal³. Conditions were then established in which single LGR5⁺ cells generate long-lived organoids that retain all characteristics of the epithelium⁴. Organoids

derived from a single adult LGR5⁺ cell were transplanted into recipient mice with chemically induced colitis, where they integrated to generate normal epithelium for at least 6 months⁵. Paneth cells provide Wnt, Notch and epidermal growth factor (EGF) signals to LGR5⁺ stem cells¹. Gene-expression profiling of sorted LGR5–GFP cells allowed us to define a short list of enriched genes, such as *Ascl2* and *Olfm4* (ref. 6). Here we address the role of two related genes that occur in this list: *Rnf43* and *Znrf3*.

We arbitrarily sorted crypt cells on the basis of LGR5–GFP expression into five fractions and performed microarray expression profiling (Supplementary Fig. 2a, b). As expected, *Lgr5* and other stem-cell genes (*Olfm4*, *Ascl2* and *Tnfrsf19*) showed an expression gradient that was highest in fraction 5+ (Fig. 1a). From this microarray experiment (Gene Expression Omnibus accession number GSE36497), we identified additional genes enriched in the 5+ fraction. Among these were two related RING-type E3 ubiquitin ligases, *Rnf43* and *Znrf3*. The encoded proteins contain an ectodomain, a single transmembrane region and a cytoplasmic RING domain (Fig. 1b and Supplementary Fig. 2c). *In situ* hybridization and quantitative reverse transcriptase (RT)–PCR confirmed expression of *Rnf43* and *Znrf3* in CBC cells (Fig. 1c, red arrows; Supplementary Fig. 2d).

We generated conditional alleles of the genes by inserting two *loxP* sites flanking the exon encoding the RING domain (Supplementary Fig. 3). The alleles were individually crossed with intestinal epithelium-specific Cre lines (*Cyp11a1-cre* or villin (*Vil*)–*creERT2*), which allow gene deletion upon β -naphthoflavone and tamoxifen administration, respectively^{7,8}. Homozygous mutants did not yield any discernible phenotype (Supplementary Fig. 4). We then generated *Rnf43 Znrf3*

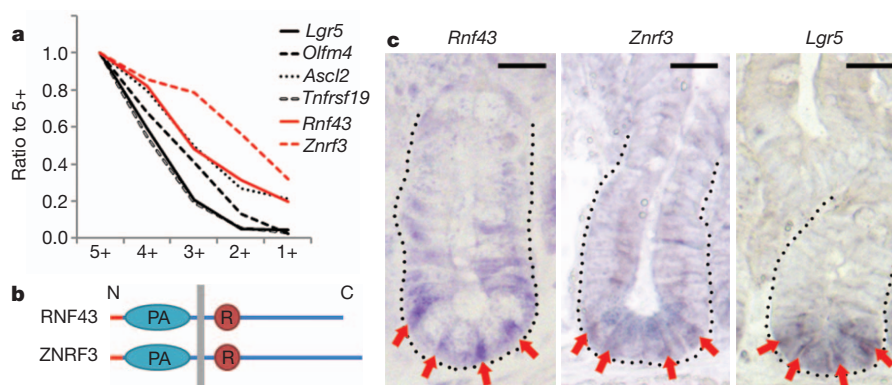


Figure 1 | LGR5⁺ stem cell genes: *Rnf43* and *Znrf3*. **a**, Graph of the expression pattern of stem-cell genes (*Lgr5*, *Olfm4*, *Ascl2* and *Tnfrsf19*) and two RING-type E3 ubiquitin ligases (*Rnf43* and *Znrf3*). Every fraction is compared to fraction 5+. **b**, Schematic overview of RNF43 and ZNRF3. The red line denotes the signal peptide and the grey line denotes the membrane. PA, protease-associated domain; R, RING domain. **c**, *In situ* hybridization of *Rnf43*, *Znrf3* and *Lgr5* in the mouse small intestinal crypt. CBC cells in between Paneth cells are indicated with red arrows. Dotted line indicates the intestinal epithelial lining of the crypt. Scale bars, 20 μ m.

protease-associated domain; R, RING domain. **c**, *In situ* hybridization of *Rnf43*, *Znrf3* and *Lgr5* in the mouse small intestinal crypt. CBC cells in between Paneth cells are indicated with red arrows. Dotted line indicates the intestinal epithelial lining of the crypt. Scale bars, 20 μ m.

¹Hubrecht Institute, KNAW and University Medical Center Utrecht, Uppsalalaan 8, 3584 CT Utrecht, The Netherlands. ²Department of Cell Biology, University Medical Center Utrecht, 3584 CX Utrecht, The Netherlands. ³Biomolecular Mass Spectrometry and Proteomics Group, Bijvoet Center for Biomolecular Research and Utrecht Institute for Pharmaceutical Sciences, Utrecht University, 3584 CH Utrecht, The Netherlands. ⁴The Netherlands Proteomics Center, Padualaan 8, 3584 CH Utrecht, The Netherlands.

*These authors contributed equally to this work.

compound mutant mice with *Vil-creERT2*. When both E3 ligases were deleted simultaneously, the mutant intestine underwent a marked expansion of the proliferative compartment (Fig. 2a, b), resembling the effects of acute deletion of *Apc*⁹. *Ki67*⁺ cells not only occupied the enlarged crypts but also appeared on the flanks of villi. The hyperproliferative cells contained high levels of β -catenin (Fig. 2d, inset), indicating a strong activation of Wnt/ β -catenin signalling such as seen upon *Apc* deletion⁹. Indeed, Wnt target genes such as *Cd44*, *Ephb2* and *Axin2* were strongly upregulated (Supplementary Fig. 5). In wild-type intestine, *Olfm4*-positive stem cells reside at crypt bottoms (Fig. 2e). In the compound mutant intestine, numbers of *Olfm4*-positive cells were strongly increased (Fig. 2f), as were the numbers of *Cryptdin6* (also known as *Defa6*)-expressing Paneth cells¹⁰ (Fig. 2h). The expansion of the stem–Paneth cell zone was confirmed by using other stem-cell (*Msi1* and *Sox9*) and Paneth cell (lysozyme) markers (Supplementary Fig. 6). Clonal deletion of *Rnf43* and *Znrf3* using a low dose of tamoxifen resulted in adenoma formation within 1 month (Fig. 2i). In the adenoma, intestinal stem cells continuously expanded while generating Paneth cells (Fig. 2j, k). We also deleted *Rnf43* and *Znrf3* stochastically in LGR5⁺ stem cells using *Lgr5-creERT2*. Again, these mutant stem cells generated adenomas that contained *Olfm4*-positive stem cells and lysozyme-positive Paneth cells, but no other differentiated cell types (Supplementary Fig. 7).

We cultured intestinal organoids from wild-type and *Rnf43 Znrf3* compound mutant mice. *Rnf43 Znrf3* compound mutant organoids grew faster than controls (Supplementary Fig. 8). R-spondin1 (RSPO1), an essential component of the medium, is a ligand of LGR5, which itself resides in the frizzled–LRP complex. Through these interactions, RSPO1 potently enhances Wnt signals^{11–13}. Whereas control organoids died within 5 days after the removal of RSPO1,

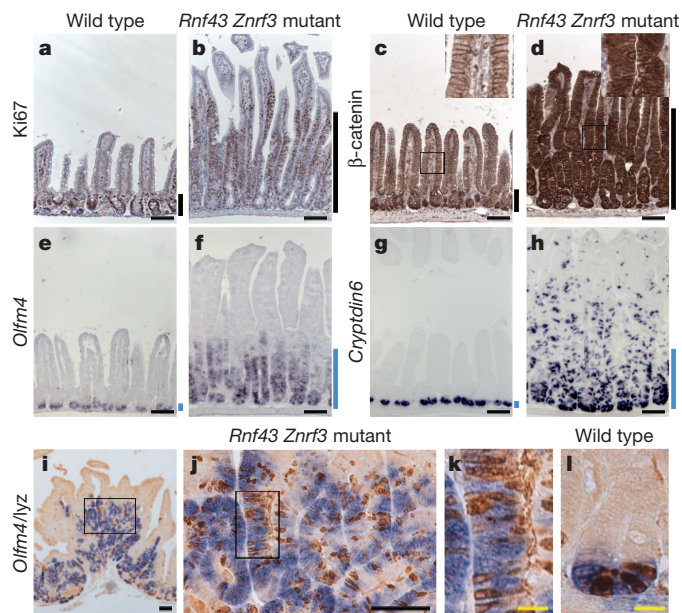


Figure 2 | Strong proliferation of the *Rnf43 Znrf3* compound mutant intestine is accompanied by Wnt/ β -catenin activation as well as stem cell and Paneth cell metaplasia. a–h, Wild-type (a, c, e and g) and *Rnf43 Znrf3* compound mutant (b, d, f and h) intestines are stained for Ki67 (a, b; for proliferating cells), β -catenin (c, d), *Olfm4* (e and f; for stem cells) and *Cryptdin6* (g, h; for Paneth cells). These intestines were analysed 1 week after tamoxifen induction (5 mg). Side bars indicate Ki67-positive proliferative zone (black) and *Olfm4*-positive stem cell zone (blue), respectively. i–l, Adenoma formation in the *Rnf43 Znrf3* compound mutant intestine. Formation of adenoma was observed 1 month after tamoxifen induction (1 mg) in *Rnf43 Znrf3* compound mutant (i–k) and wild-type mice (l). j and k are high-magnification images of boxed regions in i and j, respectively. Note that stem-cell (*Olfm4*, in blue) expansion accompanies Paneth cell metaplasia (Lyz, in brown). Lyz, lysozyme. Scale bars, 100 μ m (black) and 10 μ m (yellow).

the mutant organoids could be maintained for at least 4 weeks in the absence of RSPO1 (Supplementary Fig. 9f, i). We proposed that mutant stem cells were hypersensitive to Paneth-cell-derived WNT3, rendering them RSPO1-independent. To test this, we treated the cultures with a small molecule inhibitor of porcupine¹⁴, thus blocking the secretion of functional WNT3 by Paneth cells¹. Inhibitor treatment resulted in the death of both the wild-type and *Rnf43 Znrf3* mutant organoid cultures within 5 days, illustrating that Paneth-cell-derived WNT3 was indeed essential (Supplementary Fig. 9g, i). The effect of the inhibitor was completely rescued by exogenous WNT3A (Supplementary Fig. 9d, h). Taken together, we conclude that mutation of *Rnf43* and *Znrf3* rendered LGR5⁺ stem cells hypersensitive to locally secreted Wnt, resulting in adenoma formation *in vivo* and RSPO1-independent growth *in vitro*. Unlike *Apc*-mutant adenoma cells that activate the Wnt pathway cell autonomously, *Rnf43 Znrf3* mutant cells depend on paracrine Wnt signals for their growth.

Because RNF43 and ZNRF3 acted as negative Wnt regulators, we tested the effect of RNF43 overexpression in mouse intestinal *Vil-creERT2*-derived organoids by retroviral expression using a vector that harbours a floxed *dsRed* complementary DNA upstream of *RNF43* (ref. 15). After tamoxifen treatment, the induced RNF43 expression inhibited organoid growth immediately (Supplementary Fig. 9m). Growth could be restored with a GSK3- β inhibitor, but not by exogenous WNT3A (Supplementary Fig. 9n–p), indicating that the negative effect of RNF43 on Wnt/ β -catenin signalling occurred upstream of GSK3- β .

We also performed Wnt reporter assays in HEK293T cells transfected with either wild-type *RNF43* or *RNF43* mutants with inactivating point mutations in their RING domain (MT). A small amount of RNF43 completely abolished the response to exogenous WNT3A (Fig. 3a). A similar effect was observed after transfection of *Znrf3* (Supplementary Fig. 10). The RNF43 RING mutants showed no inhibition but instead acted in a dominant-negative manner and enhanced Wnt signalling activity (Fig. 3a). The inhibitory effect of RNF43 was not observed when the Wnt pathway was activated by dominant-active LRP6 with an amino-terminal deletion (Δ N-LRP6)¹⁶, or by a GSK3- β inhibitor (Fig. 3b), suggesting that the effect occurred at the level of the frizzled receptors for Wnt.

RNF43 mutations have been identified in two colorectal cancer cell lines containing an activating β -catenin (*CTNNB1*) mutation rather than an *APC* mutation¹⁷. HCT116 cells harbour one wild-type and one mutant *CTNNB1* allele. As a consequence, the Wnt pathway is modestly active in these cells, and can be strongly enhanced by exogenous Wnt¹⁸. We confirmed the homozygous *RNF43* mutation in HCT116 cells (Supplementary Fig. 11a). Re-expression of RNF43 in these cells blocked the effect of WNT3A (Fig. 3c). These results indicate that mutations of *RNF43* synergize with mutations in *CTNNB1* in colon cancer cells.

To assess whether RNF43 selectively controls Wnt receptor expression at the cell surface, we generated stable transfectants of HEK293 cells in which RNF43 expression could be induced by doxycycline (Dox). Cells were surface-labelled with biotin both before and 24 h after the addition of Dox, and their surface proteomes were compared by mass spectrometry. We confirmed RNF43 as the most upregulated protein on the cell surface, whereas FZD1, FZD2, FZD3 and LRP5 were among the eight most strongly downregulated surface proteins (Fig. 3d).

We next investigated how expression of RNF43 affects the subcellular distribution of frizzled proteins. To this end, we expressed a functional version of FZD5 that carried a SNAP tag in its extracellular domain. SNAP–FZD5 labelling with membrane-impermeable SNAP–Alexa549 showed its stable localization at the cell surface (Fig. 3e). After co-expression with RNF43, FZD5 was rapidly internalized (Fig. 3e). A similar effect was noted after transfection of *Znrf3* (Supplementary Fig. 10b). This was not observed when various mutants of RNF43 were co-expressed with FZD5, indicating that both RING

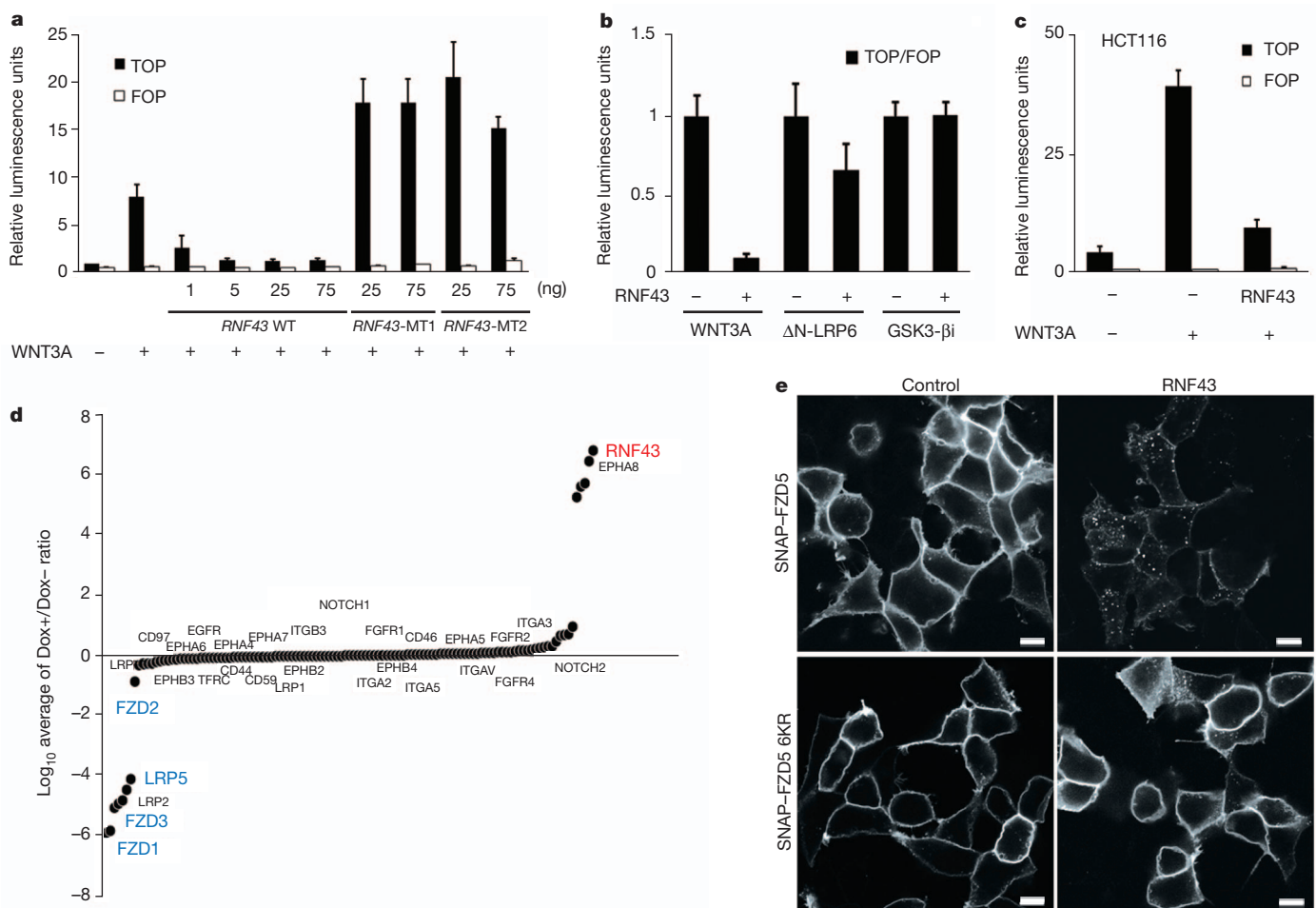


Figure 3 | RNF43 suppresses the Wnt/ β -catenin pathway by reducing surface levels of frizzled receptors. **a**, Luciferase assay of TCF4- β -catenin activity in the presence of RNF43. RNF43 abolishes WNT3A-activated luciferase activity in a dose-dependent manner. RING domain RNF43 point mutants (RNF43-MT1, C290S/H292S; RNF43-MT2, H295S/C298S) do not downregulate luciferase activity. WT, wild type. **b**, Luciferase assay of TCF4- β -catenin activity with various stimuli (WNT3A, ligand; Δ N-LRP6, active form of co-receptor; GSK3- β i, inhibitor of GSK3- β that activates signalling downstream of the Wnt receptors). RNF43 overexpression strongly suppresses WNT3A-mediated signalling whereas signalling downstream of frizzled (Δ N-LRP6 and GSK3- β i) remains unaffected. Luciferase activities are normalized to control cells. **c**, Luciferase assay of TCF4- β -catenin activity in HCT116 cells.

activity and the ectodomain are important to promote FZD5 internalization (Supplementary Fig. 11b). A non-ubiquitinatable FZD5 6KR variant (in which all cytosolic lysine residues are substituted by arginine residues) was resistant to RNF43-mediated internalization, indicating a direct role for ubiquitination (Fig. 3e). Flow cytometric analyses confirmed that RNF43 reduced surface expression of FZD5 (Supplementary Fig. 11c).

Ubiquitin modification commonly drives cell-surface receptor internalization and lysosomal degradation¹⁹. De-ubiquitination controls the recycling of receptors, including frizzled receptors²⁰. Co-expression of RNF43 strongly and selectively decreased levels of the mature, complex glycosylated form of FZD5, whereas the immature form remained unaffected (Fig. 4a and Supplementary Fig. 12a). Both the RNF43 RING domain and FZD5 lysine acceptor sites for ubiquitin were essential for this effect. Indeed, RNF43 strongly promoted ubiquitination of FZD5 (Fig. 4b). Notably, lysosomal inhibition (bafilomycin A1) counteracted the RNF43-mediated degradation of FZD5, whereas proteasomal inhibition (MG132) had no effect (Fig. 4b and Supplementary Fig. 12b). RNF43 interacted with FZD5 as assessed

Re-expression of RNF43 in HCT116 cells blocks the effect of exogenous WNT3A. **d**, Relative abundance of surface proteins detected by mass spectrometry in the presence or absence of RNF43. After induction of RNF43, surface levels of FZD1, FZD3 and LRP5 are largely reduced. **e**, Subcellular localization of SNAP-FZD5 and lysine mutant SNAP-FZD5 6KR in HEK293T cells co-transfected with control or RNF43. Surface SNAP-FZD5 was labelled with SNAP-Alexa549 for 15 min and chased for 5 min. Note that RNF43 induces rapid internalization of SNAP-FZD5. SNAP-FZD5 6KR is resistant to RNF43-induced internalization. Scale bars, 10 μ m. Error bars denote s.d., $n = 3$. Three independent biological experiments were performed for the luciferase assays (a–c). FOP, mutant negative control luciferase reporter; TOP, TCF optimal luciferase reporter.

by co-immunoprecipitation, and both proteins co-localized in internal vesicles (Fig. 4c, d). On expression of RNF43, surface FZD5 was efficiently targeted to RAB5⁺ early endosomes and CD63⁺ lysosomes (Supplementary Fig. 12c, d). We conclude that RNF43 negatively regulates Wnt/ β -catenin signalling by ubiquitinating frizzled receptors, thereby targeting this Wnt receptor to the lysosomal pathway for degradation.

Previous studies have identified *Rnf43* and *Znrf3* as target genes of the Wnt pathway^{6,21,22}. The current study demonstrates that they act as inhibitors of Wnt signalling by negatively regulating frizzled receptor surface expression. The same notion was put forward in a study²³ that appeared while the current manuscript was under revision. Thus, these genes join the class of negative-feedback Wnt pathway regulators, which includes DKK1 (ref. 24), APCDD1 (ref. 25) and AXIN2 (ref. 26). The inverse mechanism has been proposed for the Wnt receptor tyrosine kinase RYK: the ubiquitin ligase MIB1 triggers its internalization and thereby activates Wnt signalling²⁷.

Homeostasis of the intestinal stem-cell compartment is governed by a number of positive- and negative-feedback regulators of

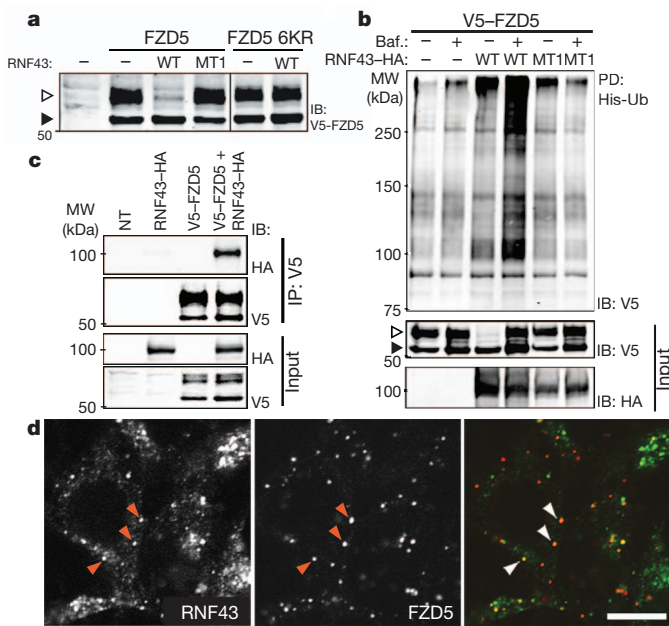


Figure 4 | RNF43 promotes ubiquitin-mediated endocytosis of frizzled receptors. **a**, RNF43 regulates FZD5 turnover. Levels of mature, complex glycosylated V5-conjugated FZD5 (V5-FZD5) are selectively downregulated in HEK293T cells co-expressing RNF43, but not mutant RNF43 (MT1). V5-FZD5 6KR levels remain unaffected by RNF43 co-expression. Arrowheads denote immature (filled) and mature (open) V5-FZD5. IB, immunoblot. **b**, RNF43 mediates ubiquitination of FZD5. HEK293T cells were transfected with V5-FZD5, His-ubiquitin and wild-type or mutant (M1) haemagglutinin-conjugated RNF43 (RNF43-HA), as indicated. Treatment of cells with bafilomycin A1 (Baf.), an inhibitor of lysosomal acidification, rescues FZD5 from RNF43-mediated downregulation (middle). Levels of ubiquitinated FZD5 (top) significantly accumulate upon RNF43 co-expression and lysosomal inhibition, but not with RNF43-MT1. Arrowheads denote immature (filled) and mature (open) V5-FZD5. PD, pull-down; Ub, ubiquitin. **c**, RNF43 interacts with FZD5. V5-FZD5 was immunoprecipitated (IP) from bafilomycin A1-treated HEK293T cells expressing V5-FZD5 and RNF43-HA, as indicated. NT, non-transfected. **d**, RNF43-GFP co-localizes with SNAP-FZD5 in internal vesicles. Surface SNAP-FZD5 was labelled with SNAP-Alexa549 for 15 min and chased for 30 min in HEK293T cells. Arrowheads indicate co-localization. Scale bars, 10 μ m.

Wnt/ β -catenin signalling^{6,12}, indicating the importance of balancing adequate levels of Wnt activity. We propose that RNF43 and ZNRF3 serve to restrict the size of the intestinal stem-cell zone. Indeed, their genetic removal leads to unrestricted expansion of the stem-cell zone in a fashion that is reminiscent of the removal of another negative Wnt pathway regulator, APC⁹. Unlike APC-mutant adenomas however, *Rnf43 Znf3* compound mutant adenomas depend on paracrine Wnt factors from Paneth cells within the mutant clone. RNF43 is a genuine tumour suppressor: it was recently found to be mutated in human intraductal papillary mucinous neoplasm, a class of pancreatic neoplasia²⁸ and in cholangiocarcinoma²⁹. *RNF43* was also found to be mutated in a transposon-based screen for intestinal adenoma formation in mice³⁰ and in two colon cancer cell lines¹⁷. Deep-sequencing efforts have shown further cases of *RNF43* mutations in colorectal and other cancers (<http://www.sanger.ac.uk/perl/genetics/CGP/cosmic?action=mutations&ln=RNF43&start=1&end=784&coords=AA:AA&neg=off&page=1>). Our findings indicate that human tumours that harbour mutations in *RNF43* may be treatable by Wnt pathway inhibitors that act at the level of Wnt secretion or receptor activation.

METHODS SUMMARY

Reagents. Murine recombinant EGF was from PeproTech. Noggin- and RSP01-conditioned media were generated from HEK293 cells. WNT3A-conditioned media was generated from L cells. Y-27632 was from Sigma. CHIR99021 was

from Stemgent. Porcupine inhibitor IWP1 was provided by L. Lum¹⁴. Endoribonuclease-prepared short interfering RNAs for *RNF43* (EHU058181) and *ZNRF3* (EHU136411) were from Sigma. N-terminal SNAP-tagged mouse FZD5 was designed on the basis of previously described V5-Fz5 (ref. 31).

Mice. *Rnf43* and *Znf3* floxed alleles were generated through homologous recombination in embryonic stem cells as described¹². Details of these constructs are available on request. Experiments were performed according to guidelines and reviewed by the Dier Experimenten Commissie (DEC) of the KNAW.

Crypt isolation, cell dissociation and culture. Crypt isolation, cell dissociation and culture have been described previously⁴. For the analysis of organoid growth under various conditions, established organoid cultures were dissociated into small pieces and seeded in Matrigel (BD Biosciences) under the appropriate growth condition. Growth morphology of organoids was imaged daily and viability of each organoid was scored.

Microarray analysis. LGR5-GFP-positive cells from *Lgr5-GFP-IRES-creERT2* knock-in intestines were sorted into five different fractions based on their GFP intensity. RNeasy Micro kit (Qiagen) was used to isolate RNA, and microarray analysis (Agilent) was performed as previously described¹. The data were deposited to the Gene Expression Omnibus (accession number GSE36497).

Full Methods and any associated references are available in the online version of the paper.

Received 23 March; accepted 11 June 2012.

Published online 15 August 2012.

- Sato, T. *et al.* Paneth cells constitute the niche for Lgr5 stem cells in intestinal crypts. *Nature* **469**, 415–418 (2011).
- Cheng, H. & Leblond, C. P. Origin, differentiation and renewal of the four main epithelial cell types in the mouse small intestine. I. Columnar cell. *Am. J. Anat.* **141**, 461–479 (1974).
- Barker, N. *et al.* Identification of stem cells in small intestine and colon by marker gene *Lgr5*. *Nature* **449**, 1003–1007 (2007).
- Sato, T. *et al.* Single Lgr5 stem cells build crypt-villus structures *in vitro* without a mesenchymal niche. *Nature* **459**, 262–265 (2009).
- Yui, S. *et al.* Functional engraftment of colon epithelium expanded *in vitro* from a single adult Lgr5⁺ stem cell. *Nature Med.* **18**, 618–623 (2012).
- van der Flier, L. G. *et al.* Transcription factor achaete scute-like 2 controls intestinal stem cell fate. *Cell* **136**, 903–912 (2009).
- El Marjou, F. *et al.* Tissue-specific and inducible Cre-mediated recombination in the gut epithelium. *Genesis* **39**, 186–193 (2004).
- Ireland, H. *et al.* Inducible cre-mediated control of gene expression in the murine gastrointestinal tract: effect of loss of β -catenin. *Gastroenterology* **126**, 1236–1246 (2004).
- Sansom, O. J. *et al.* *Myc* deletion rescues Apc deficiency in the small intestine. *Nature* **446**, 676–679 (2007).
- van Es, J. H. *et al.* Wnt signalling induces maturation of Paneth cells in intestinal crypts. *Nature Cell Biol.* **7**, 381–386 (2005).
- Carmon, K. S., Gong, X., Lin, Q., Thomas, A. & Liu, Q. R-spondins function as ligands of the orphan receptors LGR4 and LGR5 to regulate Wnt/ β -catenin signaling. *Proc. Natl Acad. Sci. USA* **108**, 11452–11457 (2011).
- de Lau, W. *et al.* Lgr5 homologues associate with Wnt receptors and mediate R-spondin signalling. *Nature* **476**, 293–297 (2011).
- Kazanskaya, O. *et al.* The Wnt signaling regulator R-spondin 3 promotes angioblast and vascular development. *Development* **135**, 3655–3664 (2008).
- Chen, B. *et al.* Small molecule-mediated disruption of Wnt-dependent signaling in tissue regeneration and cancer. *Nature Chem. Biol.* **5**, 100–107 (2009).
- Koo, B. K. *et al.* Controlled gene expression in primary Lgr5 organoid cultures. *Nature Methods* **9**, 81–83 (2012).
- Liu, G., Bafico, A., Harris, V. K. & Aaronson, S. A. A novel mechanism for Wnt activation of canonical signaling through the LRP6 receptor. *Mol. Cell. Biol.* **23**, 5825–5835 (2003).
- Ivanov, I., Lo, K. C., Hawthorn, L., Cowell, J. K. & Ionov, Y. Identifying candidate colon cancer tumor suppressor genes using inhibition of nonsense-mediated mRNA decay in colon cancer cells. *Oncogene* **26**, 2873–2884 (2007).
- Li, V. S. *et al.* Wnt signaling through inhibition of β -catenin degradation in an intact Axin1 complex. *Cell* **149**, 1245–1256 (2012).
- Haglund, K. & Dikic, I. The role of ubiquitylation in receptor endocytosis and endosomal sorting. *J. Cell Sci.* **125**, 265–275 (2012).
- Mukai, A. *et al.* Balanced ubiquitylation and deubiquitylation of Frizzled regulate cellular responsiveness to Wg/Wnt. *EMBO J.* **29**, 2114–2125 (2010).
- Van der Flier, L. G. *et al.* The intestinal Wnt/TCF signature. *Gastroenterology* **132**, 628–632 (2007).
- Yagyu, R. *et al.* A novel oncoprotein RNF43 functions in an autocrine manner in colorectal cancer. *Int. J. Oncol.* **25**, 1343–1348 (2004).
- Hao, H. X. *et al.* ZNRF3 promotes Wnt receptor turnover in an R-spondin-sensitive manner. *Nature* **485**, 195–200 (2012).
- Niida, A. *et al.* DKK1, a negative regulator of Wnt signaling, is a target of the β -catenin/TCF pathway. *Oncogene* **23**, 8520–8526 (2004).
- Shimomura, Y. *et al.* APCDD1 is a novel Wnt inhibitor mutated in hereditary hypotrichosis simplex. *Nature* **464**, 1043–1047 (2010).

26. Jho, E. H. *et al.* Wnt/ β -catenin/Tcf signaling induces the transcription of Axin2, a negative regulator of the signaling pathway. *Mol. Cell Biol.* **22**, 1172–1183 (2002).
27. Berndt, J. D. *et al.* Mindbomb 1, an E3 ubiquitin ligase, forms a complex with RYK to activate Wnt/ β -catenin signaling. *J. Cell Biol.* **194**, 737–750 (2011).
28. Wu, J. *et al.* Whole-exome sequencing of neoplastic cysts of the pancreas reveals recurrent mutations in components of ubiquitin-dependent pathways. *Proc. Natl Acad. Sci. USA* **108**, 21188–21193 (2011).
29. Ong, C. K. *et al.* Exome sequencing of liver fluke-associated cholangiocarcinoma. *Nature Genet.* **44**, 690–693 (2012).
30. March, H. N. *et al.* Insertional mutagenesis identifies multiple networks of cooperating genes driving intestinal tumorigenesis. *Nature Genet.* **43**, 1202–1209 (2011).
31. Tauriello, D. V. *et al.* Loss of the tumor suppressor CYLD enhances Wnt/ β -catenin signaling through K63-linked ubiquitination of Dvl. *Mol. Cell* **37**, 607–619 (2010).

Supplementary Information is linked to the online version of the paper at www.nature.com/nature.

Acknowledgements We thank A. A. Rolf, I. Kuper, M. van den Born, C. Kroon-Veenboer, H. Begthel, J. Korving and S. van den Brink for technical assistance, L. Lum for providing

IWP1 and S. Bartfeld for the schematic drawing. This work was funded in part by grants from the European Research Council, EU/232814-StemCellMark and the National Research Foundation of Korea, NRF-2011-357-C00093 (B.-K.K.); EU/Health-F4-2007-200720 (M.v.d.W.); The Centre van Biomedical Genetics (D.E.S.); Ti Pharma/T3-106 (J.H.v.E.); the European Research Council, ERC-StG no.242958 (M.M.M.) and the KNAW/3V-fund.

Author Contributions B.-K.K., M.M.M. and H.C. conceived and designed the experiments. B.-K.K., M.S., I.J., D.E.S., M.v.d.W. and J.H.v.E. performed the experiments. T.Y.L., S.M. and A.J.R.H. performed the mass spectrometry analysis. B.-K.K., M.S., I.J., M.M.M. and H.C. analysed the data. B.-K.K., M.M.M. and H.C. wrote the manuscript.

Author Information The data for the microarray analysis have been deposited to the Gene Expression Omnibus under accession number GSE36497. Reprints and permissions information is available at www.nature.com/reprints. The authors declare competing financial interests: details accompany the full-text HTML version of the paper at www.nature.com/nature. Readers are welcome to comment on the online version of this article at www.nature.com/nature. Correspondence and requests for materials should be addressed to M.M.M. (M.M.Maurice@umcutrecht.nl) or H.C. (h.clevers@hubrecht.eu).

METHODS

Plasmids. N-terminal SNAP-tagged mature mouse FZD5 (Ala27-Val559) was generated by PCR-subcloning SNAP from nSNAP (Bioke) between mouse H2-Kb signal sequence and FZD5 as described for V5-Fz5³¹. SNAP-FZD5 6KR was generated by substitution of cytoplasmic lysines 347, 434, 439, 442, 445 and 525 for arginines by site-directed mutagenesis. RNF43-2×Flag-HA and RNF43-GFP constructs were generated by PCR-subcloning. His-ubiquitin was a gift from B. Burgering.

Histology, immunohistochemistry and *in situ* hybridization. Mouse intestine was fixed in 4% paraformaldehyde and embedded in paraffin. For immunohistochemistry, the primary antibodies were mouse anti-Ki67 (1:250, Monosan), mouse anti- β -catenin (1:100, BD Transduction Laboratories) and rabbit anti-lysozyme (1:1,500, DAKO). For *in situ* hybridization, digoxigenin (DIG)-labelled complementary RNA probes were generated from cDNA-containing vectors (from IMAGE consortium or RZPD) by *in vitro* transcription.

Surface biotinylation and mass spectrometry analysis. Surface proteins from Dox-inducible RNF43-overexpressing HEK293 cells were enriched by using EZ-Link Sulfo-NHS-SS-Biotin, (Thermo Fisher) according to manufacturer's protocol, except for the following modifications. After intensive washing, the resin was rinsed with five volumes of PBS buffer to remove residual detergent. Biotinylated proteins were eluted after 1 h incubation, once with 5 mM dithiothreitol (DTT), and 0.5% RapiGest SF surfactant (Waters) in 50 mM ammonium bicarbonate, and twice with 5 mM DTT and 8 M urea in 50 mM ammonium bicarbonate. Each elution was stored separately. All samples were subjected to alkylation with iodoacetamide (in the dark at room temperature for 20 min) followed by digestion with Lys-C and then trypsin overnight. RapiGest detergent was precipitated by addition of 5% trifluoroacetic acid and removed by centrifugation. Digested samples were pooled and desalted with SEP-PAK C18 (Waters) before vacuum-drying.

Each sample was analysed in triplicates by performing nano-ultra performance liquid chromatography (LC)-tandem mass spectrometry (MS/MS) on a Proxeon EASY-nLC 1000 (Thermo Scientific) connected to a LTQ-Orbitrap Q-Exactive (Thermo Fisher Scientific). The injected sample was first trapped with a double-fritted trapping column (Dr Maisch Reprosil C18, 3 μ m, 2 cm \times 100 μ m) before being separated in an analytical column (Agilent Zorbax SB-C18, 1.8 μ m, 35 cm \times 50 μ m). Solvent A consisted of 0.1 M acetic acid and solvent B consisted of 0.1 M acetic acid in 80% acetonitrile. Measurement time for each sample took 240 min. Samples were first loaded at a maximum pressure of 980 bar with 100% solvent A. Subsequently, peptides were chromatographically separated by a 211 min gradient consisting of 10–40% solvent B at a flow of 100 nl min⁻¹; then ramped to 100% solvent B in 3 min and held in 100% solvent B for another 2 min. This was finally followed by a 13 min equilibration with 100% solvent A. For MS analysis, 1.7 kV was applied to the nano-spray needle. The survey scan was from 350 to 1500 *m/z* at a resolution of 30,000 and for MS/MS the resolution was set to 7500. The 20 most intense precursors were selected for fragmentation with higher energy dissociation. The target ion setting was 3E6 for MS and 5E4 for MS/MS, with a maximum fill-time of 250 ms and 120 ms, respectively.

Protein identification and extracted ion chromatogram detection. The raw files were converted to peak lists using Proteome Discoverer version 1.3 (Thermo Fisher Scientific) and searched against IPI (International Protein Index) human database version 3.37 (69,164 sequences; 29,064,824 residues) using Mascot search engine (version 2.3.02; <http://www.matrixscience.com>), with trypsin set as the enzyme. The database search was made with the following parameters set to consider a peptide tolerance of \pm 50 p.p.m., a fragment tolerance of \pm 0.02 Da allowing two missed cleavages, carbamidomethyl as a fixed modification and oxidation and protein N-terminal acetylation as variable modifications. The results were then filtered using Percolator to a false discovery rate below 1%. Filtered peptides assigned with a Mascot score lower than 20 were discarded. Using Proteome Discoverer, the selected ion chromatogram for all detected peptide precursors were computed and 'top 3' strategy was used for each protein in order to provide protein areas used for subsequent label-free quantification. These raw areas were then normalized with respect to the total intensity observed

in each LC-MS analysis and against the sum of all analyses. Ultimately, a ratio was obtained by dividing the normalized area for each protein in the Dox⁺ experiment by the Dox⁻ experiment.

Immunofluorescence and ubiquitination analysis. HEK293T cells were cultured in RPMI (Invitrogen), supplemented with 10% FBS (Sigma), 100 U ml⁻¹ penicillin, and 100 μ g ml⁻¹ streptomycin and transfected with FuGENE 6 (Promega) according to the manufacturer's instructions. Bafilomycin A1 (10 nM; overnight) was used to block lysosomal acidification.

For microscopy analysis, HEK293T cells were grown on laminin-coated glass coverslips. Cells were transfected and after 20 h labelled with 1 μ M SNAP-Alexa549 (Bioke) for 15 min at room temperature. Subsequently, cells were chased for 5 or 15 min at 37 °C and fixed in 4% paraformaldehyde. Cells were incubated with mouse anti-HA (Roche), followed by secondary antibodies conjugated to Alexa488 or -680 (Invitrogen). Cells were mounted in ProLong Gold (Invitrogen) and visualized using a Zeiss LSM510 confocal microscope.

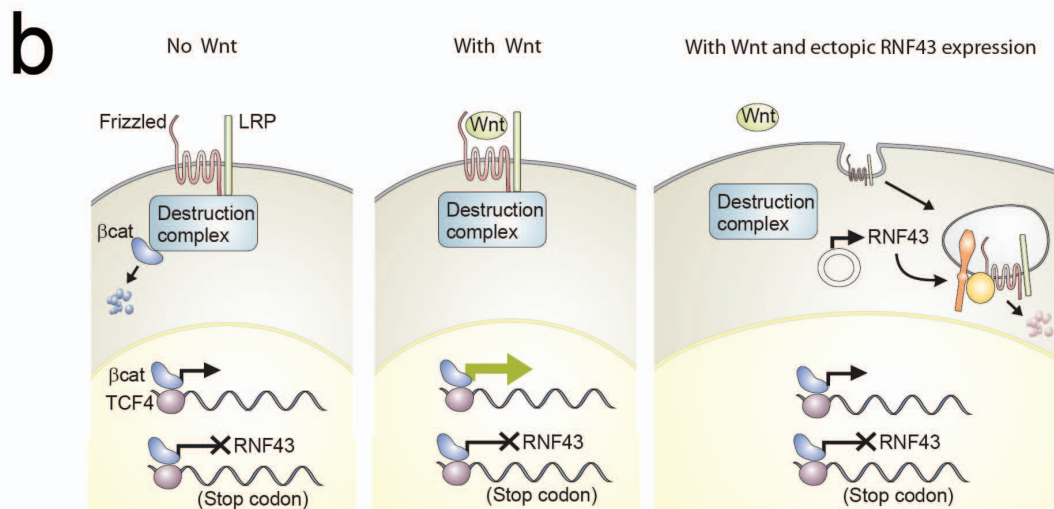
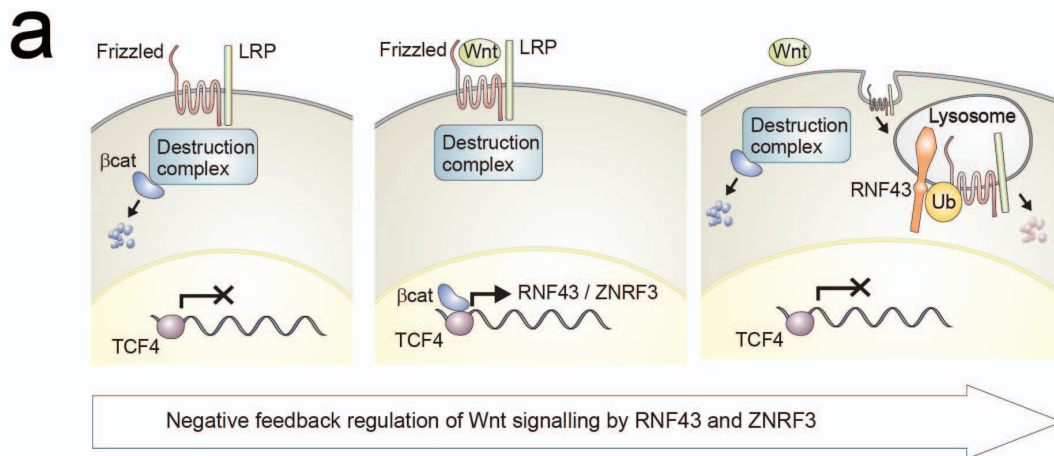
Ubiquitination analysis was done as described³¹. In brief, HEK293T cells were transfected with His-ubiquitin and V5-tagged FZD5 for 24 h, washed and collected in ice-cold PBS with 10 mM *N*-ethyl maleimide (Sigma). Cells were lysed in a chaotropic lysis buffer containing 6 M guanidinium-HCl (Fluka), 100 mM phosphate buffer, 10 mM Tris-HCl, pH 8.0, 20 mM imidazole and 10 mM β -mercaptoethanol. After sonication, lysates were cleared by centrifugation and incubated with nickel-nitrilotriacetic acid-agarose beads (Qiagen) for 2.5 h at room temperature. Beads were washed with lysis buffer with 0.2% Triton X-100, followed by sequential washes with buffers A, B and C (A, 8 M urea, 100 mM phosphate buffer, 10 mM Tris-HCl, pH 8.0, 10 mM β -mercaptoethanol and 0.2% Triton X-100; B, as buffer A, but pH 6.3; C, as B, but with 0.1% Triton X-100). His-tagged proteins were eluted with two bead volumes of elution buffer (6.2 M urea, 10 mM Tris-HCl, pH 7.0, 100 mM P buffer and 200 mM imidazole and sample buffer). For immunoblotting, rabbit anti-V5 (Sigma) and rat anti-HA (Roche) and were used. Secondary antibodies were obtained from Invitrogen.

Immunoprecipitation. HEK293T cells were co-transfected with V5-FZD5 and mock plasmid or RNF43-HA, and treated with bafilomycin A1 (10 nM; overnight). Cells were washed and collected in ice-cold PBS and lysed in lysis buffer (50 mM Tris, pH 7.5, 150 mM NaCl, 0.5% Triton X-100, 5 mM EDTA, 1 mM DTT, 50 mM sodium fluoride and protease inhibitors) for 20 min on ice followed by 30 min centrifugation at 4 °C. Immunoprecipitations were performed on the supernatant with mouse anti-V5 (Invitrogen) and protein A beads (Repligen) for 2 h at 4 °C. Beads were washed six times with lysis buffer and proteins were eluted in \times 1.5 sample buffer.

Flow cytometric analysis. HEK293 cells with Dox-inducible RNF43 or RNF43-MT1 were transfected with V5-FZD5 and V5-FZD5 6KR. Murine stem cell virus-enhanced GFP was co-transfected to gate transfected cells. Experimental groups were treated with Dox to induce RNF43 or RNF43-MT1 expression 24 h after transfection. Dox-treated and untreated cells were collected after 12 h of incubation. Cells were washed with PBS and resuspended in FACS buffer (PBS with 1% FBS). Cells were labelled with mouse anti-V5 antibody followed by anti-mouse Alexa647 antibody. Cells were washed twice with PBS and analysed using a BD FACSCalibur. Levels of V5 were analysed for GFP-positive cells.

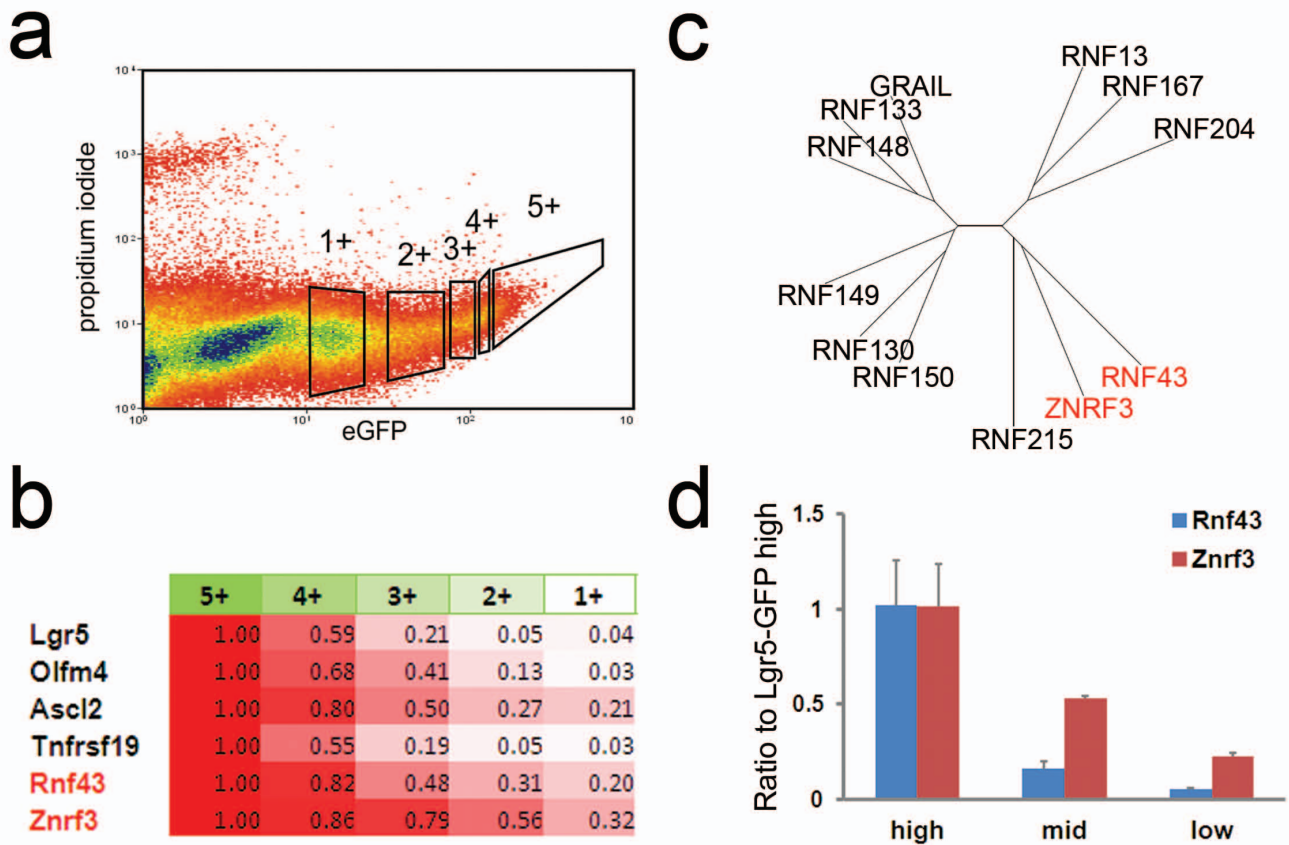
Proteasomal inhibition. HEK293T cells co-expressing V5-FZD5 and RNF43-HA were treated with vehicle (ethanol) or the proteasomal inhibitor MG132 (20 \times μ M) for 3 h before cells were lysed.

Pulse chase. HEK293T cells expressing V5-FZD5 were grown in depletion medium (-Met/-Cys) for 30 min at 37 °C. Next, medium was exchanged with labelling medium (100 μ Ci ³⁵S-Met/³⁵S-Cys per ml, Redivue, GE Healthcare) for 15 min at 37 °C. After the pulse, medium was washed away and replaced by RPMI with 10% FCS at 37 °C for the indicated time points. Subsequently, cells were washed with PBS with 10 mM *N*-ethyl maleimide and lysed in lysis buffer. Immunoprecipitation of V5-FZD5 was performed as described above. Samples were applied to SDS-PAGE, the gel was dried and a phosphorimager screen (Molecular Dynamics) was used to measure radioactivity with a Storm scanner (Amersham BioSciences).

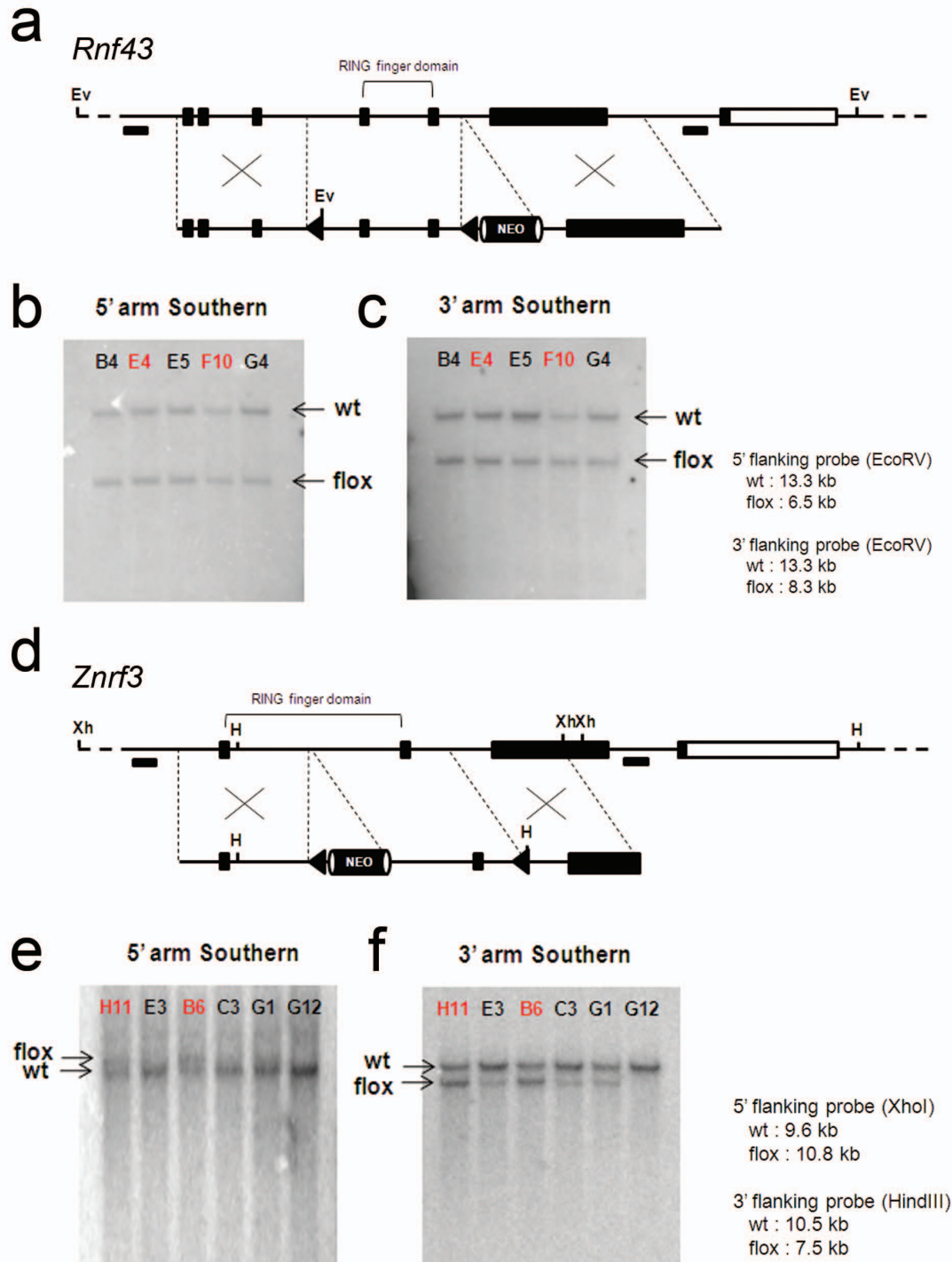


HCT116 cell line: β -catenin 1 wt, 1 mutant allele (constitutively active). RNF43 both alleles have frame shift mutation.

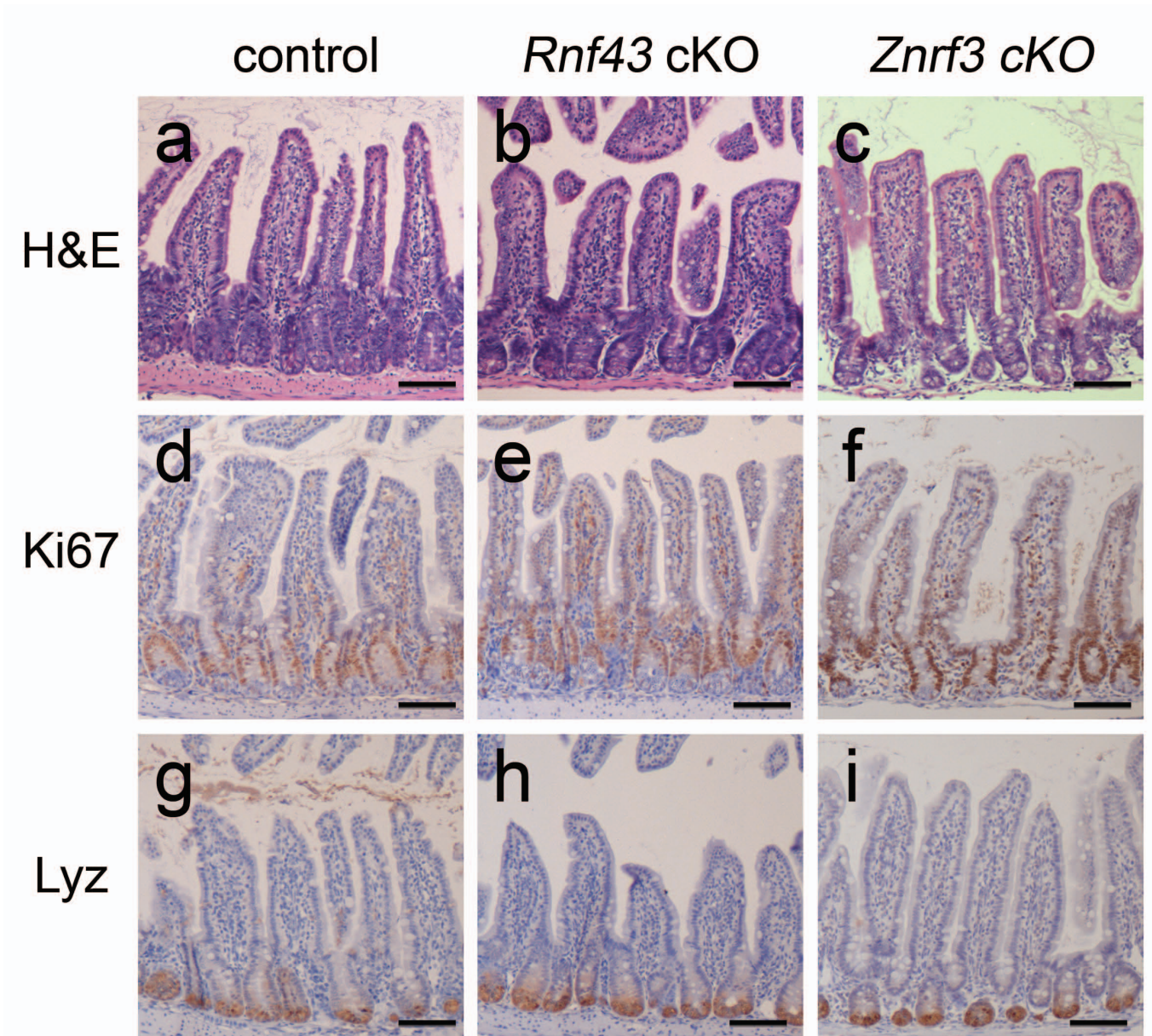
Supplementary Figure 1 | Model of negative feedback regulation of the Wnt pathway by RNF43 and ZNRF3. **a**, Left, in the resting stage, the destruction complex degrades cytosolic β -catenin thereby preventing downstream gene activation. Middle, upon Wnt stimulation, Frizzled and LRP5/6 receptors bind and inactivate the destruction complex, which leads to the accumulation of β -catenin and its migration to the nucleus. The formation of a nuclear TCF/ β -catenin complex induces gene expression of RNF43 and ZNRF3. Right, the transmembrane E3 ligases RNF43 and ZNRF3 ubiquitinate Frizzled at the plasma membrane and, consequently, promote its endocytosis and lysosomal degradation. The decrease of Frizzled receptors at the cell surface renders the cell insensitive to Wnt stimulation. **b**, Left, HCT116 cells carry one wild-type allele and one mutated, constitutively active allele of β -catenin, while expression of both RNF43 alleles is lost due to frame shift mutations. The active form of β -catenin sustains a basal level of Wnt activation in HCT116 cells. Middle, upon Wnt stimulation, significantly enhanced levels of Wnt activation are achieved due to the lack of negative feedback mediated by RNF43. Right, ectopic expression of RNF43 in HCT116 results in low level of Wnt activation.



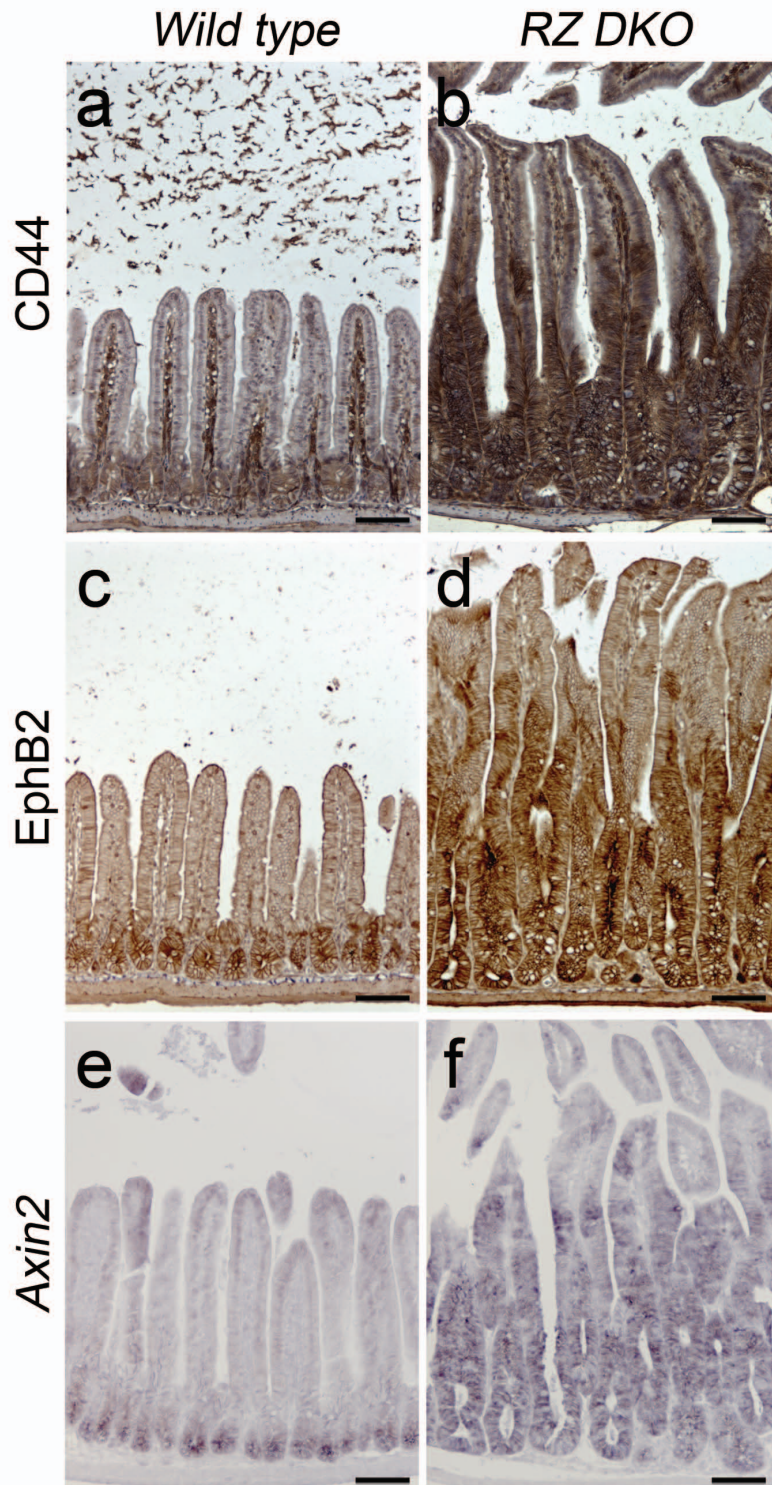
Supplementary Figure 2 | Intestinal Lgr5 stem cell-specific expression of *Rnf43* and *Znrf3*. **a**, Dot plot of flow cytometric analysis indicating the gates for each fraction of Lgr5-GFP-positive cells. Each fraction is labelled from GFP-highest (5+) to GFP-lowest (1+). Propidium iodide is used to exclude dead cells. **b**, Summary of the expression pattern of stem cell genes (*Lgr5*, *Olfm4*, *Ascl2* and *Tnfrsf19*) and two RING-type E3 ubiquitin ligases (*Rnf43* and *Znrf3*). Every fraction is compared to fraction 5+. Note that the expression levels of *Rnf43* and *Znrf3* follow the expression pattern of other stem cell genes. **c**, Phylogenetic tree of 12 PA-TM-RING (PA, PA domain; TM, transmembrane; RING, RING domain) proteins in human. RNF43 and ZNRF3 are two closely related paralogues among the 12 members. **d**, Quantitative RT-PCR for *Rnf43* and *Znrf3*. Based on the intensity of GFP expression, Lgr5-GFP high, middle (mid) and low cells were isolated. Error bar: s.d., n=3. Three technical replicates for the quantitative RT-PCR result (d).



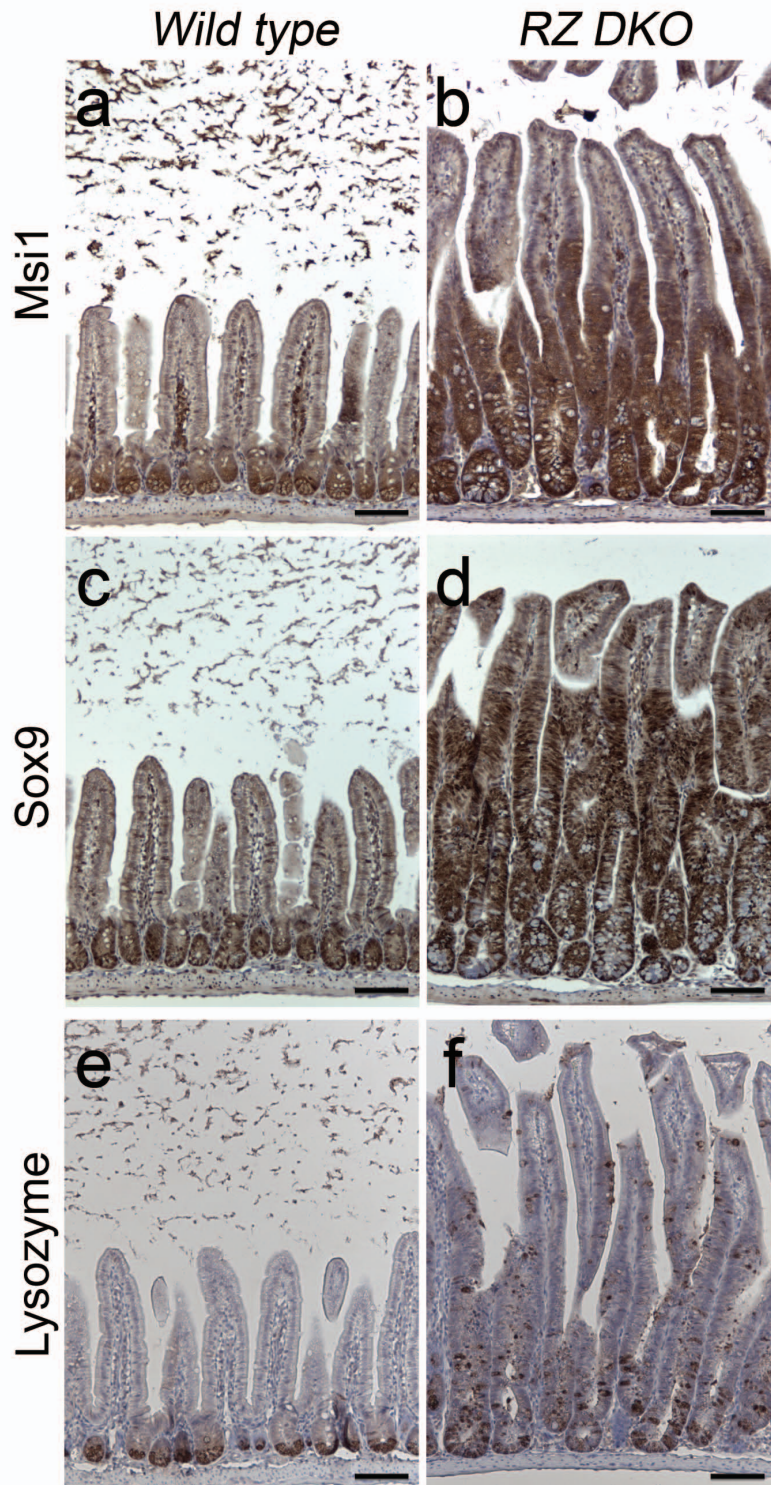
Supplementary Figure 3| Targeting strategy of *Rnf43* and *Znrf3*. **a**, Schematic overview of the *Rnf43* targeting strategy. Two exons encoding the RING domain of *Rnf43* are flanked by LoxP sites. **b**, **c**. Southern blot analysis of targeted clones with 5' flanking probe (**b**) and 3' flanking probe (**c**). The restriction enzyme used for the analysis and the expected size of the bands are indicated. **d**, Schematic overview of the *Znrf3* targeting strategy. One of the two exons encoding the RING domain of *Znrf3* is flanked by LoxP sites. **e**, **f**. Southern blot analysis of targeted clones with 5' flanking probe (**e**) and 3' flanking probe (**f**). The restriction enzymes used for the analysis and the expected size of bands are indicated. Clones indicated in red were used to generate chimeric mice to get the *Rnf43* and *Znrf3* conditional alleles.



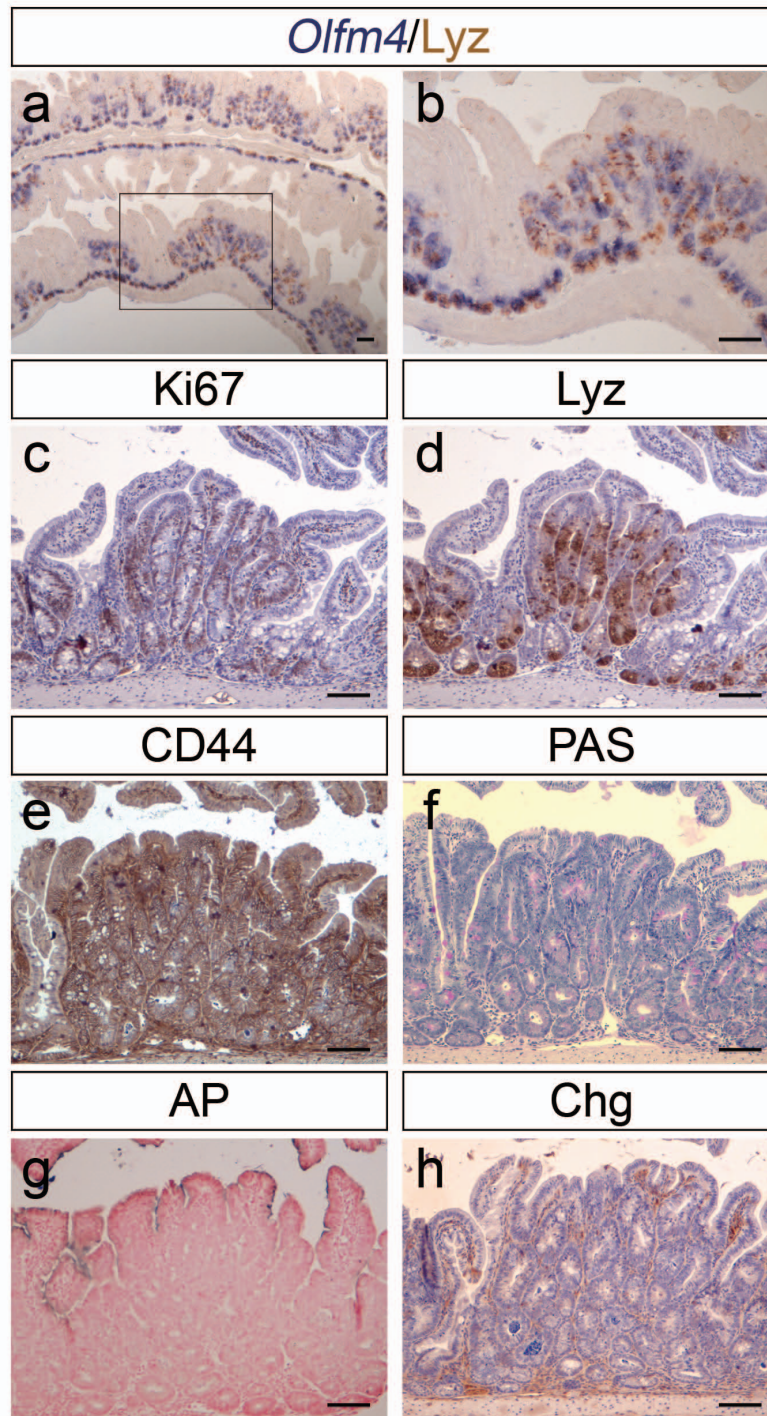
Supplementary Figure 4 | No discernible phenotype of *Rnf43* and *Znrf3* single mutants. a-i, *Wild type* (control; a, d and g), *Rnf43* conditional mutant (*Rnf43* cKO; b, e and h) and *Znrf3* conditional mutant (*Znrf3* cKO; c, f, and i) intestinal sections are stained for H&E (a, b, and c), Ki67 (d, e, and f, for proliferating cells) and Lysozyme (Lyz) (g, h, and i, for Paneth cells). Note that the number of proliferating cells and Paneth cells are comparable between different genotypes. Scale bar: 50 μ m.



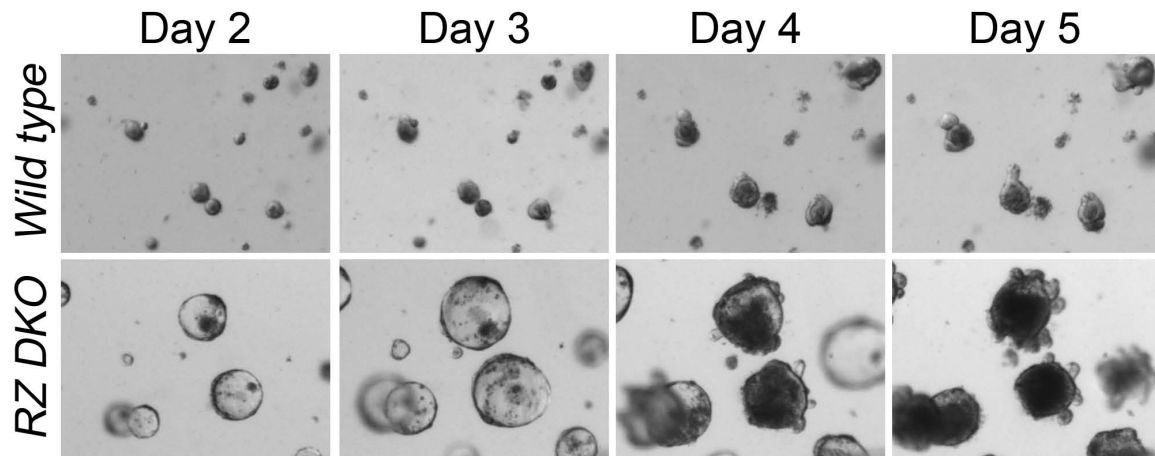
Supplementary Figure 5 | Strong activation of Wnt target gene expression in *Rnf43;Znrf3* compound mutant. a-f, Wild type (a, c and e) and *Rnf43;Znrf3* compound mutant (RZ DKO) (b, d and f) intestinal sections are stained for Wnt-target genes, CD44 (a and b), EphB2 (c and d) and *Axin2* (e and f). Scale bar: 100 μ m.



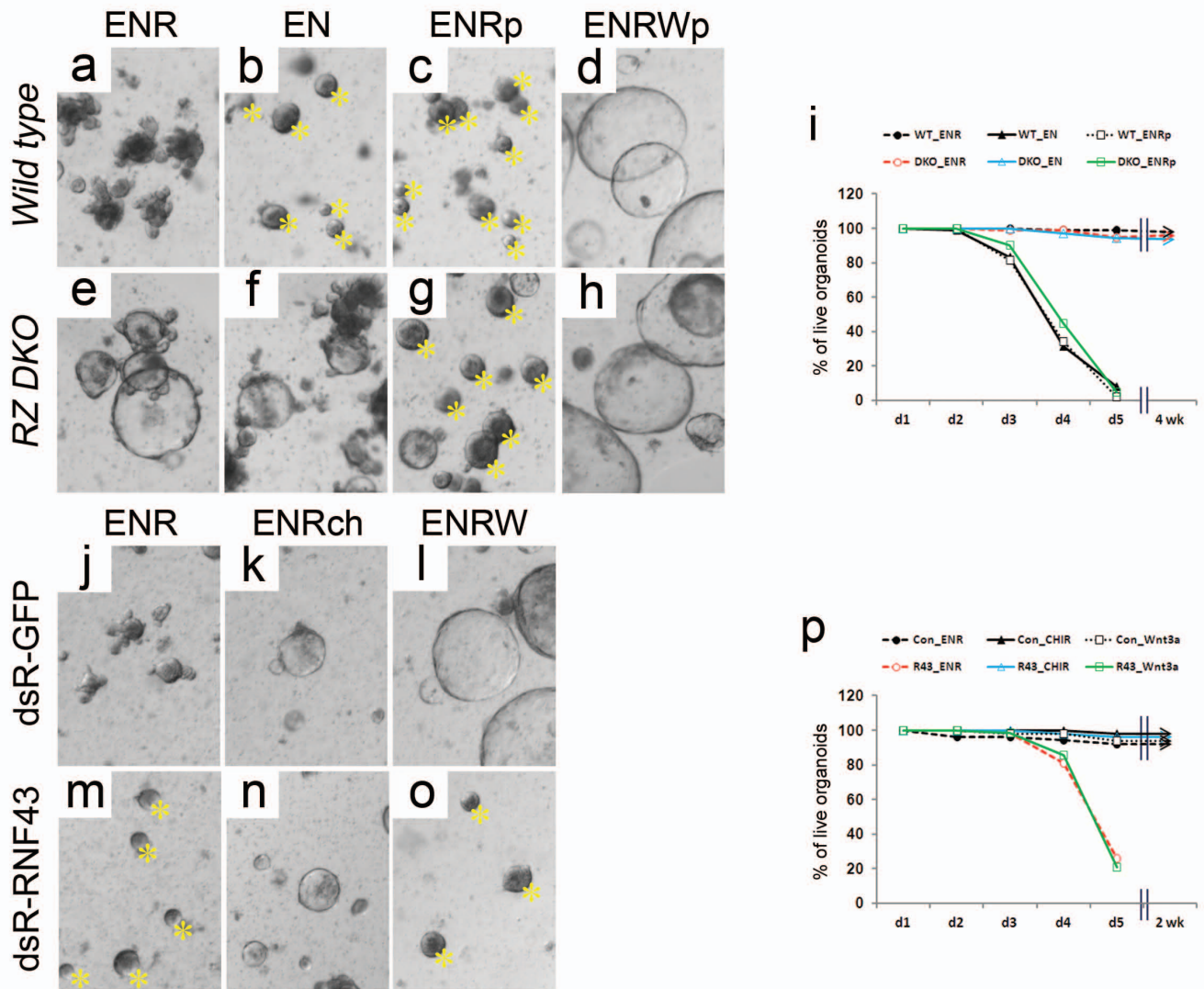
Supplementary Figure 6 | Increased number of progenitors and Paneth cells in *Rnf43;Znrf3* compound mutant. a-f, Wild type (a, c and e) and *Rnf43;Znrf3* compound mutant (RZ DKO) (b, d and f) intestinal sections are stained for progenitor cell markers, Msi1 (a and b) and Sox9 (c and d), and the Paneth cell marker, Lysozyme (e and f). Scale bar: 100 μ m.



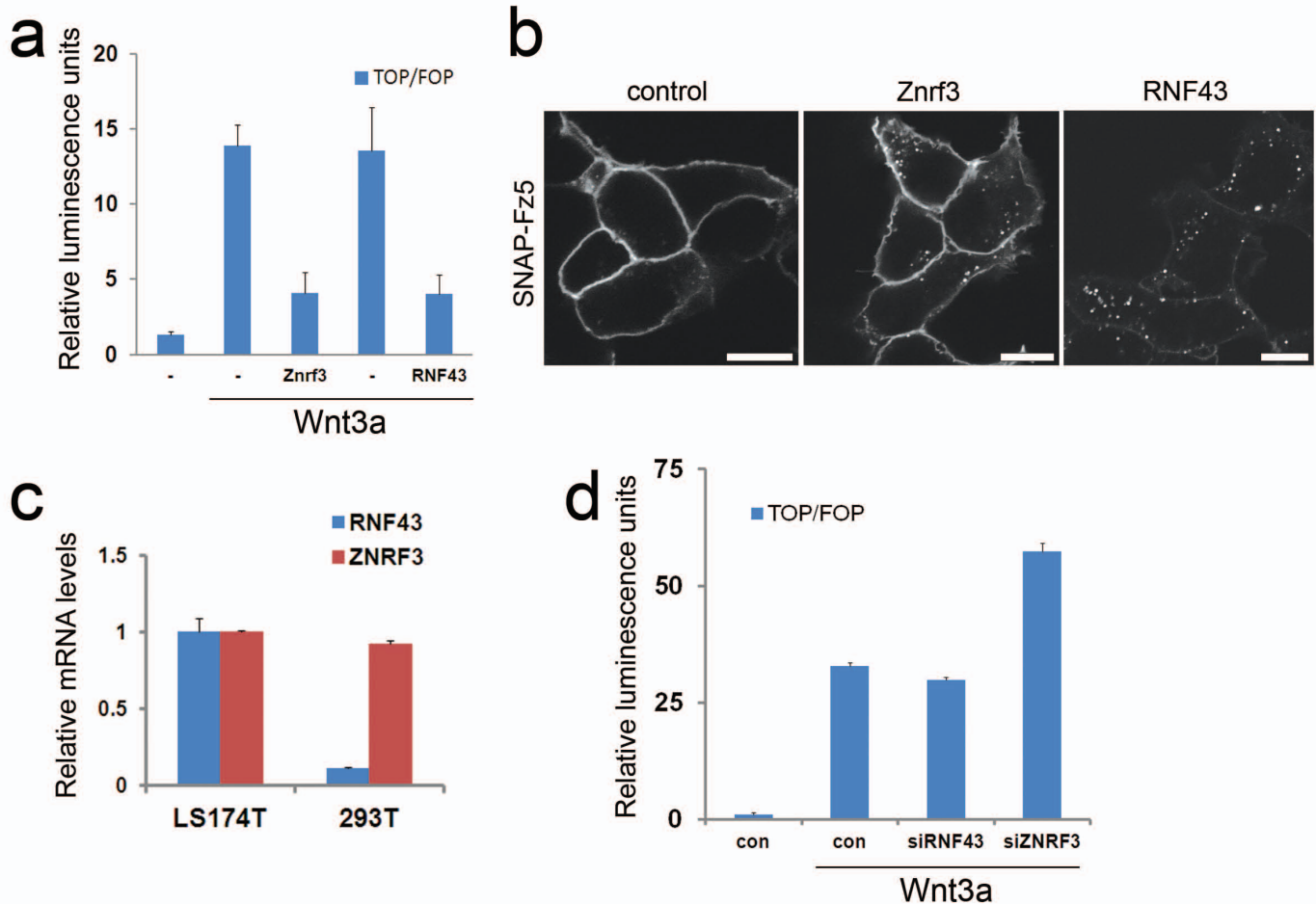
Supplementary Figure 7 | Clonal deletion of *Rnf43* and *Znrf3* in *Lgr5* stem cells results in intestinal polyposis. a-h, Multiple adenomas are formed in *Lgr5-GFPiresCreER;Rnf43;Znrf3* compound mutant intestine after tamoxifen induction. Formation of adenoma was observed one month after tamoxifen treatment. Adenomas are stained for *Olfm4* (blue, for stem cells) and Lysozyme (Lyz, brown, for Paneth cells) (a, b), Ki67 (c, for proliferating cells), Lyz (d, for Paneth cells), CD44 (e, for Wnt-active cells), PAS (f, for goblet cells), Alkaline phosphatase (AP, g, for enterocytes), and Chromogranin (Chg, for enteroendocrine cells). b shows a high magnification image of the rectangled region in a. Note that adenomas mainly consist of proliferating progenitor/stem cells and Paneth cells. Scale bar: 100 μ m.



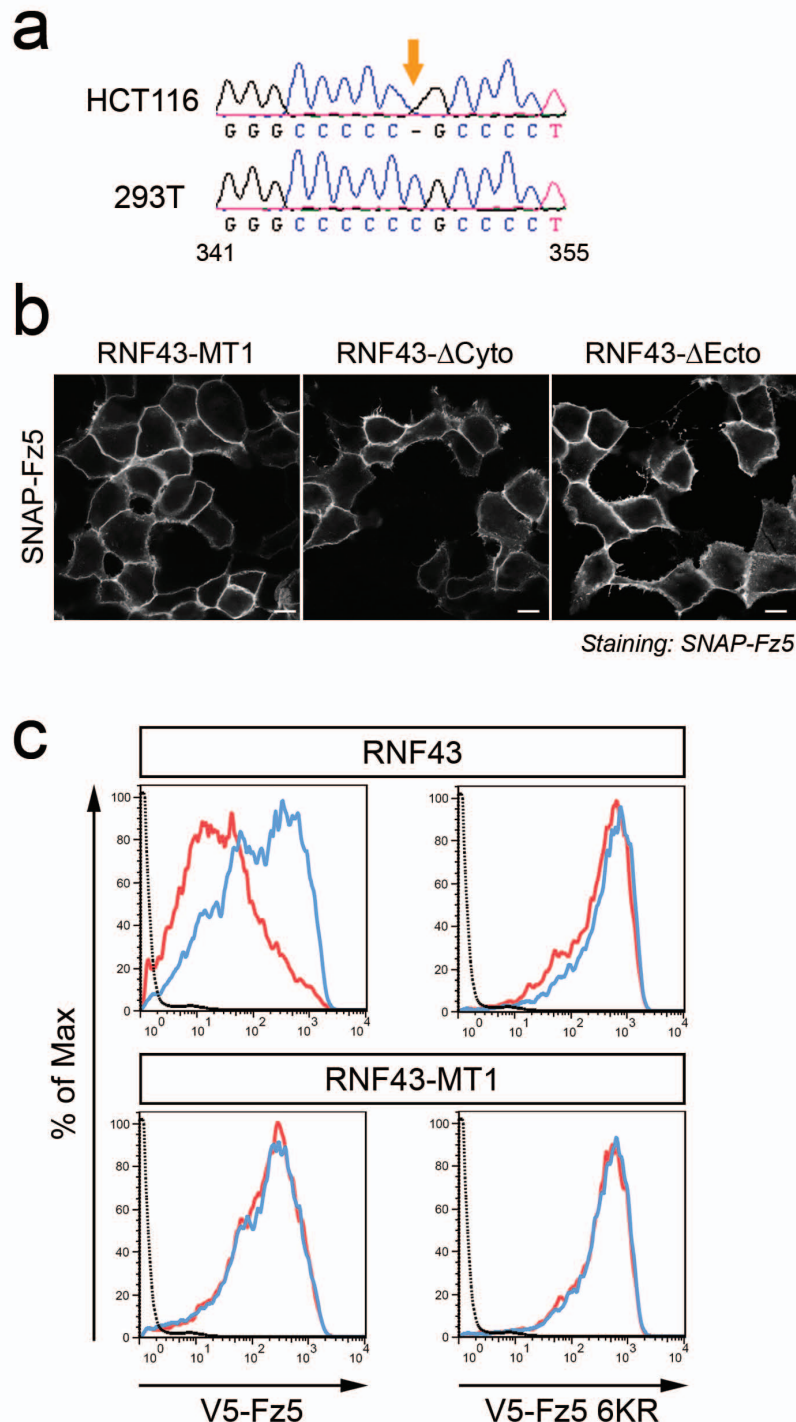
Supplementary Figure 8 | Growth of organoids. *Wild type* and *RZ DKO* organoids under normal growth conditions containing Egf, Noggin and Rspo1. Note that *RZ DKO* organoids grow significantly faster than control organoids.



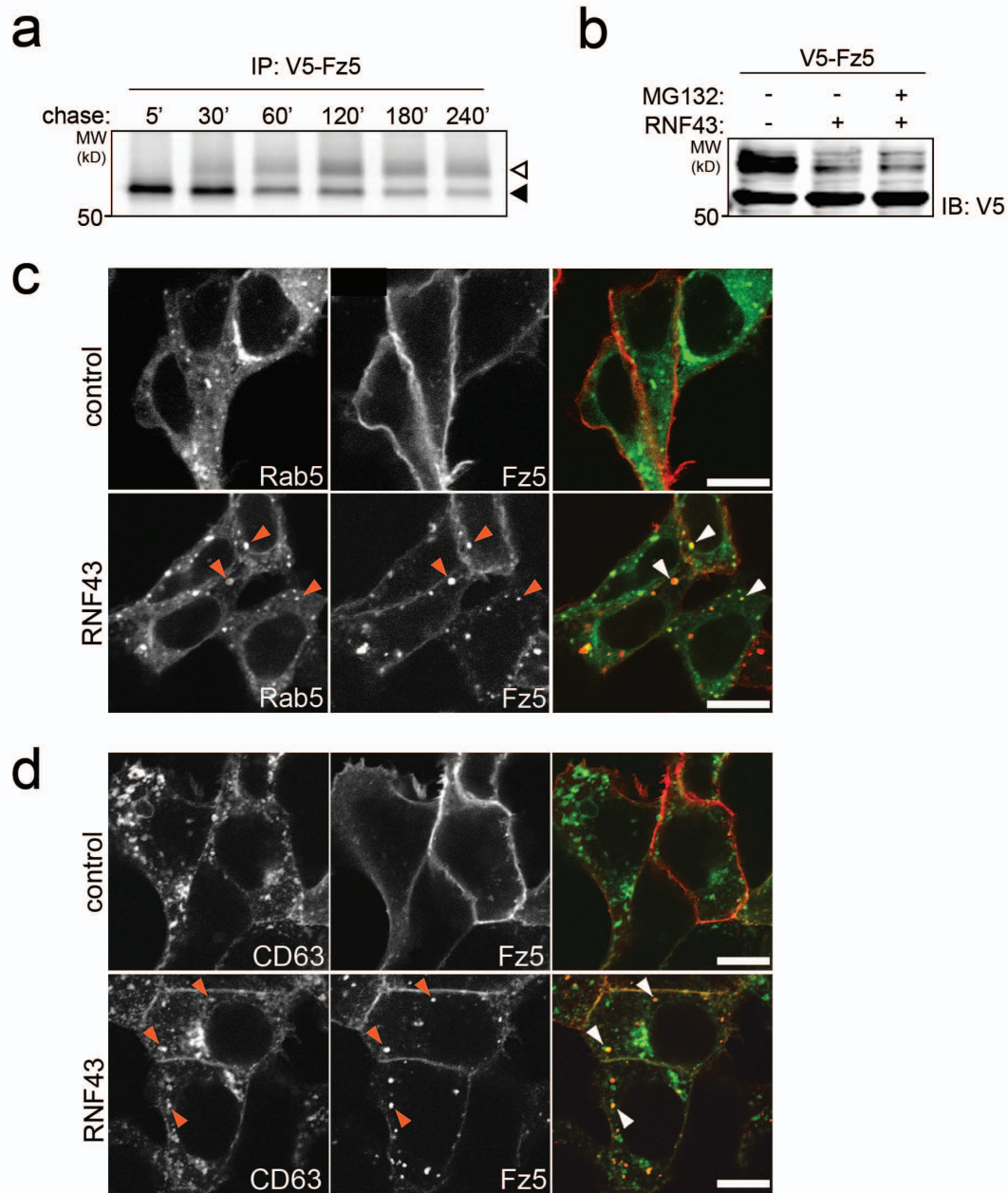
Supplementary Figure 9| *In vitro* phenotyping using organoids. **a-h**, *Wild type* (a, b, c and d) and *RZ DKO* (e, f, g and h) organoids under various growth conditions (E, Egf; N, Noggin; R, Rspo1; p, porcupine inhibitor (IWP1) and W, Wnt3a). Note that *RZ DKO* organoids grow in the absence of Rspo1. Asterisks indicate dying organoids on day 3 which were confirmed to be dead on day 5. **i**, Survival curve of organoids in each condition. Arrow indicates that organoids in the condition can grow for >4 weeks. **j-o**, DsR-GFP (j, k and l; control) and dsR-RNF43 (m, n and o) overexpressing organoids under various growth conditions (ch, GSK3 β inhibitor (CHIR99021) and W, Wnt3a). Note that RNF43 overexpression-mediated growth arrest is restored by inhibiting GSK3 β . Asterisks indicate dying organoids on day 3 which were confirmed to be dead on day 5. **p**, Survival curve of organoids in each condition. Arrow indicates that organoids in the condition can grow for >2 weeks. The average of two biological replicates is shown (i and p).



Supplementary Figure 10 | Znr3 has a similar function to RNF43. **a**, Luciferase assay of TCF4- β -catenin activity in the presence of Znr3 and RNF43. Both Znr3 and RNF43 abolish Wnt3a-activated luciferase activity in HEK293T cells. **b**, Subcellular localisation of SNAP-Fz5 in the absence or presence of Znr3-HA or RNF43-HA in HEK293T cells. Surface SNAP-Fz5 was labelled with SNAP-Alexa⁵⁴⁹ for 15 minutes and chased for 15 minutes. Scale bars 10 μ m. **c**, Quantitative RT-PCR for *RNF43* and *ZNRF3* in LS174T colon cancer cells and HEK293T cells. **d**, Luciferase assay of TCF4- β -catenin activity upon knockdown of ZNRF3 and RNF43 by esiRNA. Depletion of ZNRF3 in HEK293 cells induces a modest enhancement of Wnt signalling activity. Error bar: s.d., n=3. Three independent biological experiments were performed for the luciferase assays (a and d) and three technical replicates for the quantitative RT-PCR result (c).



Supplementary Figure 11| Both RING activity and the ecto-domain of RNF43 are important to promote Fz5 internalisation. **a**, Frame shift mutation in *RNF43* in HCT116 cells. **b**, Subcellular localisation of SNAP-Frizzled-5 (SNAP-Fz5) in HEK293T cells co-transfected with RNF43-mutants (RNF43-MT1, ligase dead point mutant; RNF43- Δ Cyto, deletion of the cytoplasmic portion; RNF43- Δ Ecto, deletion of the extracellular portion) as indicated. Scale bars 10 μ m. **c**, Flowcytometric analysis of HEK293 cells with doxycycline (Dox)-inducible RNF43 and RNF43-MT1 expressing V5-Fz5 and V5-Fz5 6KR. RNF43 decreases surface levels of Fz5. Blue line, Dox (-); Red line, Dox (+); Dotted line, untransfected cells.



Supplementary Figure 12 | RNF43 triggers endocytosis of Fz5. **a**, Complex glycosylated Fz5 is derived of a lower MW immature Fz5 form. HEK293T cells expressing V5-Fz5 were pulse-labeled with [³⁵S]methionine for 15 min and chased for the indicated time-points. Between 30-120 min chase, the mature complex glycosylated form of Fz5 gradually increases, while the immature form decreases over time. Arrowheads: immature (filled) and mature (open) V5-Fz5. **b**, Down regulation of mature V5-Fz5 levels by RNF43 cannot be rescued by proteasomal inhibition. HEK293T cells co-expressing V5-Fz5 and RNF43-HA were treated either with vehicle or the proteasomal inhibitor MG132 (20uM) for 3 hours. **c**, RNF43 targets SNAP-Fz5 to Rab5+ endosomes. Subcellular localisation of SNAP-Fz5 and GFP-Rab5 in HEK293T cells in the absence or presence of RNF43. **d**, RNF43 targets SNAP-Fz5 to CD63+ lysosomes. Subcellular localisation of SNAP-Fz5 and CD63-GFP in HEK293T cells in the absence or presence of RNF43. Surface SNAP-Fz5 was labelled with SNAP-Alexa⁵⁴⁹ for 15 minutes and chased for 5 minutes. Arrowheads indicate co-localisation. Scale bars 10 μ m.